

Exoplanet Occurrence Rates from Microlensing Surveys

Przemek Mróz and Radosław Poleski

Abstract The number of exoplanets detected using gravitational microlensing technique is currently larger than 200, which enables population studies. Microlensing is uniquely sensitive to low-mass planets orbiting at separations of several astronomical units, a parameter space that is not accessible to other planet-detection techniques, as well as free-floating planets, not orbiting around any star. In this review, we present the state-of-the-art knowledge on the demographics of exoplanets detected with microlensing, with a particular emphasis on their occurrence rates. We also summarize the current knowledge about free-floating planets, an elusive population of objects that seem to be more common than ordinary, gravitationally bound exoplanets.

Introduction

Since the inception of an idea that extrasolar planets may be detected with gravitational microlensing more than 30 years ago by Mao and Paczyński (1991) and Gould and Loeb (1992), microlensing surveys have discovered over 200 exoplanets (as shown in Fig. 1), and this number is expected to substantially increase in the upcoming years. Microlensing is unique among exoplanet-detection techniques, as it enables us to discover cold low-mass planets orbiting far from their host stars, which are largely inaccessible to other planet-detection methods. Microlensing is also unique because it is a transient phenomenon; we can infer properties of the

Przemek Mróz
Astronomical Observatory, University of Warsaw, Al. Ujazdowskie 4, 00-478 Warszawa, Poland,
e-mail: pmroz@astrouw.edu.pl

Radosław Poleski
Astronomical Observatory, University of Warsaw, Al. Ujazdowskie 4, 00-478 Warszawa, Poland,
e-mail: rpoleski@astrouw.edu.pl

Authors contributed equally.

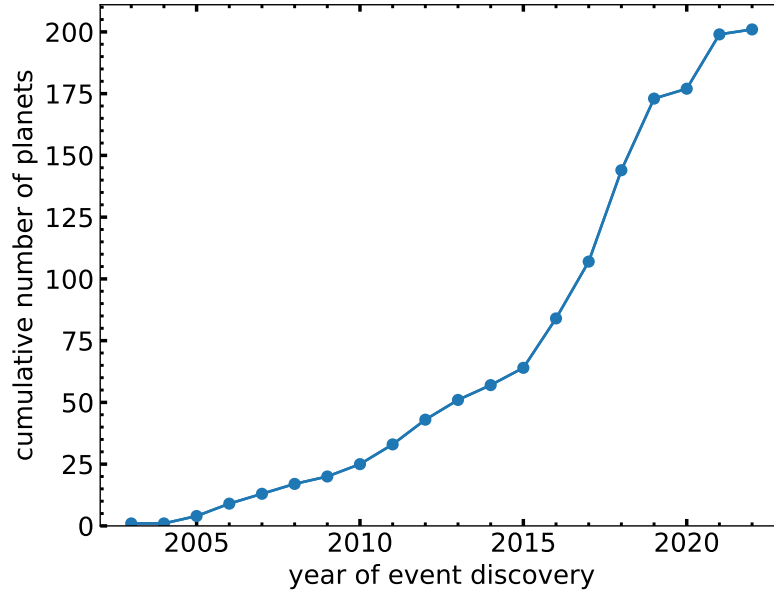


Fig. 1 Cumulative number of known extrasolar planets detected with gravitational microlensing as a function of the event discovery year. The number of planets detected per year increases in 2011 and 2016, when large-scale surveys started: OGLE-IV and KMTNet, respectively. The smaller number of planets in the last few years is caused by the telescopes shutdown due to pandemic (2020) and the publication bias (2021 and 2022). Data were taken from the NASA Exoplanet Archive (accessed 09/08/2023).

planet from the available data, but the opportunities for the follow-up observations are restricted. Therefore, microlensing surveys for exoplanets are especially suited for studying their demographics, most importantly, measuring the exoplanet occurrence rates.

Gravitational microlensing is the effect predicted by Einstein’s theory of general relativity. It occurs when light from a distant background star (called “source”) is deflected by the gravitational field of an intervening object (called “lens”). If the lens is an isolated body, usually two images of the source star are created. These images cannot normally be resolved with traditional telescopes, but their combined brightness is larger than the brightness of the source when unlensed (i.e., the source is magnified). The relative motion of the observer, the lens, and the source causes the total magnification to vary in time, producing a characteristic light curve of a microlensing event (Paczynski 1986).

If the lens is orbited by a planet and the planet happens to be located in the vicinity of one of the images created by microlensing, the planet may induce a short-lasting anomaly in an otherwise smooth light curve of the event. By modeling the shape of the light curve, it is possible to measure two parameters that describe the planet-star system: q – the planet to star mass ratio and s – the projected separation relative to the angular Einstein ring radius θ_E . The latter quantity defines the char-

acteristic angular scale of the event and depends on the mass of the lens M and the relative lens-source parallax π_{rel} :

$$\theta_E = \sqrt{\kappa M \pi_{\text{rel}}} = 0.5 \text{ mas} \left(\frac{M}{0.3 M_\odot} \right)^{1/2} \left(\frac{\pi_{\text{rel}}}{0.1 \text{ mas}} \right)^{1/2}, \quad (1)$$

where $\kappa = 4G/c^2 \text{ au} = 8.144 \text{ mas } M_\odot^{-1}$ is a constant and $\pi_{\text{rel}} = \text{au}/D_1 - \text{au}/D_s$, where D_1 and D_s are distances to the lens and the source, respectively. Microlensing is most sensitive to planets located near the Einstein ring, that is, at a separation of between 1 and 5 au (Fig. 2) for typical configurations in the Milky Way. The peak sensitivity coincides with the location of the snow line, a region in the protoplanetary disk where the majority of planets are thought to be formed (e.g., Ida and Lin 2004).

Additional information is required for translating parameters of the microlensing model (s, q) to physical parameters of the system, such as the projected star-planet separation a_\perp or the mass of the planet m_p . This information can be obtained from the so-called second-order effects in microlensing light curves. The finite-source effects (Gould 1994; Nemiroff and Wickramasinghe 1994; Witt and Mao 1994), which are detectable in the most of planetary microlensing events, enable one to measure the angular Einstein radius (see Yoo et al. (2004) for the practical implementation of the method). The microlensing parallax effects (Gould 1992) yield the parameter $\pi_E \equiv \pi_{\text{rel}}/\theta_E$. The microlensing parallax can be measured in either long-duration events, in which the orbital motion of the Earth around the Sun induces small deviations in the microlensing light curve, or events observed simultaneously from two separated observatories. Then, the mass of the lens can be estimated directly:

$$M = \frac{\theta_E}{\kappa \pi_E}, \quad (2)$$

and the mass of the planet is simply

$$m_p = \frac{qM}{1+q}. \quad (3)$$

The distance to the planetary system can be inferred based on definitions of π_{rel} and π_E :

$$\frac{\text{au}}{D_1} = \theta_E \pi_E + \frac{\text{au}}{D_s}. \quad (4)$$

Additionally, the mass and distance to the lens can sometimes be inferred when the light from the lens (host star) is directly detected in high-resolution images taken several years after the event, when the lens and the source separate in the sky (e.g., Alcock et al. 2001; Bennett et al. 2015; Batista et al. 2015).

Once we know the distance to the lens, the value of s can be translated to a 2D separation in physical units $a_\perp = sD_1\theta_E$. The deprojection of a_\perp from a 2D separation to a full 3D separation is even more complicated. It can be done in rare cases of triple lenses (one planet plus two stars or two planets orbiting one star) using orbital stability considerations (Madsen and Zhu 2019). An alternative de-

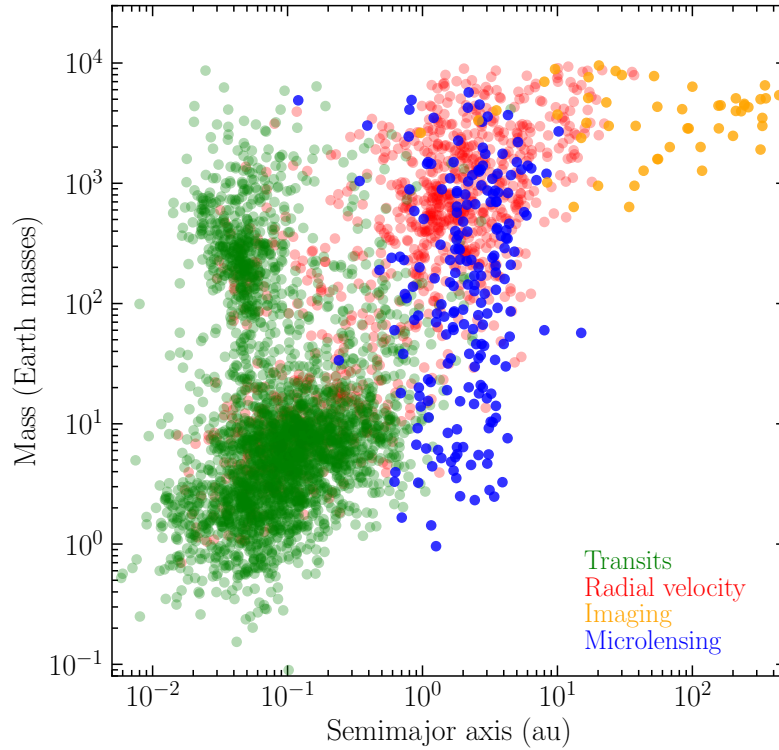


Fig. 2 Properties of known exoplanets in mass vs. semi-major axis plane. Color codes the detection technique: green—transits, red—radial velocity, orange—direct imaging, blue—microlensing. Data were taken from the NASA Exoplanet Archive (accessed 09/08/2023).

projection method is to measure the orbital motion of the planet during the event with an accuracy high enough that the full Keplerian orbit has to be considered. So far, this technique has been used only in the case of star-star lenses (e.g., Skowron et al. 2011; Wyrzykowski et al. 2020), which light curves show longer anomalies. A de-projection method that can be always applied is to statistically guess the de-projection factor based on the assumption of a random position of the planet on its orbit, but this approach has a limited value.

We refer the reader to reviews by Gaudi (2012), Gould (2016b), and Batista (2018) for a detailed description of the phenomenology of planetary microlensing events and the methods used to characterize the exoplanets detected.

Microlensing surveys

Modern experiments looking for gravitational microlensing events target mostly the dense regions of the Galactic bulge, where the chances of observing microlensing are highest. These projects repeatedly image large areas around the Galactic center, measuring the brightness of hundreds of millions stars at a cadence as short as several minutes. The Optical Gravitational Lensing Experiment (OGLE) is the longest-running microlensing survey, it has been observing the sky since 1992. The project is currently in its fourth phase (since 2010), in which it uses a mosaic camera with a field of view of 1.4 deg^2 , mounted on a 1.3-m Warsaw Telescope, located at the Las Campanas Observatory, Chile (Udalski et al. 2015). The Microlensing Observations in Astrophysics (MOA) (Sumi et al. 2003) carries out a microlensing survey with a 1.8-m MOA-II telescope, which has a 2.18 deg^2 field of view, located at the Mt. John University Observatory, New Zealand. The newest survey, the Korea Microlensing Telescope Network (KMTNet; Kim et al. 2016), uses three identical 1.8-m telescopes, each equipped with a $2^\circ \times 2^\circ$ camera. The KMTNet telescopes are located at the Cerro Tololo Inter-American Observatory (Chile), the Siding Spring Observatory (Australia), and the South African Astronomical Observatory (South Africa). Apart from these dedicated surveys, an increasing number of microlensing events (including planetary events) is detected with large all-sky surveys, such as the *Gaia* satellite (Wyrzykowski et al. 2023; Wu et al. 2023), the Zwicky Transient Facility (Rodriguez et al. 2022; Medford et al. 2023), or the All Sky Automated Survey for SuperNovae (ASAS-SN; e.g., Fukui et al. 2019).

Occurrence Rates of Bound Planets

Theory of microlensing occurrence rates

The intrinsic properties of lensing planetary systems are typically derived based on the (s, q) parameters of detected planets and the detection efficiency of the survey from which these detections come from. The detection efficiency of a survey S as a function of (s, q) is defined as the expected number of planets to be discovered if every lensing star had a planet with a given (s, q) .

There are two general approaches for estimating detection efficiency for a single event, which were presented by Gaudi and Sackett (2000) and Rhie et al. (2000). The latter method is much more frequently used than the former one. Similar to the analysis of planetary events, one has to assume what is the angle between the projected binary axis and the trajectory of the source (α). For a given event and (s, q, α) , a synthetic light curve is created with the same times of observations and the same noise properties as the original light curve. In the method of Gaudi and Sackett (2000), a binary-lens model (with fixed values of s , q , and α) is fitted to the synthetic data, and the difference $\Delta\chi^2$ is calculated between the best-fit binary-

lens model and the best-fit single-lens model. In the method of Rhie et al. (2000), a single-lens model is fitted to the synthetic data, and the difference $\Delta\chi^2$ is calculated between the best-fit single-lens model to the synthetic data and the best-fit single-lens model to the original data. The anomaly is considered as detected if $\Delta\chi^2$ is greater than some threshold value and other conditions are met (e.g., the number of anomalous epochs is larger than a threshold value). The $\Delta\chi^2$ threshold used by different authors varies between 60 and 500 (see references in Udalski et al. 2018).

The above strategy allows checking if the planet would be detected for given (s, q, α) parameters. To obtain the detection efficiency for the event i and a given pair (s, q) , i.e., $S_i(s, q)$, one simulates a grid of uniformly spaced α values and sets $S_i(s, q)$ to be the number of possible detections divided by the number of the grid points. Then one obtains the survey detection efficiency by summing the detection efficiencies over all the events analyzed: $S(s, q) = \sum_i S_i(s, q)$.

An important aspect of the detection efficiency calculations is the assumed value of the normalized source radius:

$$\rho = \frac{\theta_*}{\theta_E} = 0.013 \left(\frac{\theta_*}{6.3 \mu\text{as}} \right) \left(\frac{M}{0.3 M_\odot} \right)^{-1/2} \left(\frac{\pi_{\text{rel}}}{0.1 \text{mas}} \right)^{-1/2}, \quad (5)$$

where $6.3 \mu\text{as}$ is the angular radius of a red clump star (i.e., $11 R_\odot$) located in the Galactic center. The value of ρ can significantly affect almost all light curves in which planets can be detected, yet, this parameter is rarely constrained for single-lens events, which are used for detection efficiency calculations. If the finite-source effects are detected, then a smaller ρ generally results in a higher amplitude and a shorter duration of the anomaly than a larger ρ .

So far, the approaches used to estimate ρ varied significantly in assumptions used. The source brightness derived from the light curve fit can be combined with the angular Einstein radius θ_E expected from a Galactic density and kinematics model (based on the event position and timescale t_E). Some authors have used the most likely output from this procedure and calculated $S_i(s, q)$ assuming that value of ρ (Gaudi et al. 2002). A more advanced approach is to take into account the uncertainty in ρ , which was done either by using three values: $\rho - \sigma_\rho$, ρ , and $\rho + \sigma_\rho$ (e.g., Suzuki et al. 2016), or taking at least a few samples and weighting them using the importance sampling technique (ten samples in the case of Poleski et al. 2021). Both above approaches sample ρ by independently sampling values of θ_* and θ_E and then calculating their ratio. In rare cases, such procedures lead to the results that are not self-consistent: it may happen that the calculated ρ is large enough for finite source effects to be visible, even though this effect is not seen in the light curve. Other problem may be the lens flux that is brighter than the observed unmagnified flux. In order to overcome these issues, one could fit the light curve together with baseline fluxes using the model that has all important physical parameters (D_l , D_s , M etc.) in addition to the parameters of the microlensing light curve. Such a fit can be done using Bayesian approach and priors on many parameters from Galactic models, stellar isochrones, and color–surface brightness relations.

The final result of the considerations presented here is the occurrence rate defined as a number of planets per star per dex of s and q , i.e.,

$$f(s, q) = \frac{d^2 N}{d \log s d \log q}. \quad (6)$$

Similarly, the occurrence rate can be defined for other variables, for example, $f(q) = dN/d \log q$.

The occurrence rate $f(s, q)$ is derived from the properties of the sample of N_{obs} detected planets $\{s_i, q_i\}$ and the survey detection efficiency. We parameterize $f(s, q)$ using a vector of parameters \mathbf{p} (for example, power-law exponents) and derive these parameters using the Bayesian techniques and likelihood (i.e., the probability of obtaining a set of $\{s_i, q_i\}$ data given parameters \mathbf{p}) defined as:

$$\mathcal{L}(\{s_i, q_i\}; \mathbf{p}) = e^{-N_{\text{exp}}(\mathbf{p})} \prod_{i=1}^{N_{\text{obs}}} f(s_i, q_i; \mathbf{p}) S(s_i, q_i), \quad (7)$$

where $N_{\text{exp}}(\mathbf{p})$ is the number of expected detections:

$$N_{\text{exp}}(\mathbf{p}) = \int f(s, q; \mathbf{p}) S(s, q) d \log s d \log q \quad (8)$$

and the integration is done over the same domain of (s, q) as searched for planets. The Eq. (7) can be derived by dividing the domain of $f(s, q)$ into bins, assuming the number of planets detected in each bin follows the Poisson distribution, and calculating the limiting case of infinitesimally small bins (i.e., bins with either zero or one planet detected).

The studies aimed at deriving the planet frequency first presented the detection efficiency for single events (e.g., Rhie et al. 2000; Kubas et al. 2008). Later, the detection efficiency was studied for a statistically significant number of events (Gaudi et al. 2002; Snodgrass et al. 2004; Tsapras et al. 2016). Finally, the microlensing planet occurrence rate was first estimated quantitatively by Sumi et al. (2010). They used ten microlensing planets known at that time and detection efficiency estimated (but not derived in detail) to be $S(q) \propto q^{0.6 \pm 0.1}$. Based on these pieces of information, only the power law index of the mass-ratio function was derived: $dN/d \log q \propto q^{-0.68 \pm 0.20}$. Because of the simplified assumptions about the detection efficiency, the normalization of the mass-ratio function could not be derived.

We present planet occurrence rates derived from microlensing data in Table 1. Some of the studies presented there are also described in more detail below. Note that different studies present occurrence rates as a function of different variables and the usage of results from previous investigations.

Table 1 Bound planet occurrence rates

Reference	n_{pl}^a	n_{ev}^b	Result ^c	Comments
Sumi et al. (2010)	10	–	$f(q) \propto q^{-0.68 \pm 0.20}$	
Gould et al. (2010)	6	13	$f(s, q) = 0.36 \pm 0.15$	for $q = 5 \times 10^{-3}$
Cassan et al. (2012)	3	440	$f(a, m_p) = 10^{-0.62 \pm 0.22} \times \left(\frac{m_p}{M_{\text{Sat}}}\right)^{-0.73 \pm 0.17}$	
Shvartzvald et al. (2016)	9	224	$f(q) \propto q^{-0.50 \pm 0.17}$	for $q < 10^{-1.4}$; the slope is 0.32 ± 0.38 for larger q
Suzuki et al. (2016)	22	1474	$f(s, q) = 0.61_{-0.16}^{+0.21} \times s^{0.49 \pm 0.48} \left(\frac{q}{1.7 \times 10^{-4}}\right)^{-0.93 \pm 0.13}$	q exponent changes to $0.6_{-0.4}^{+0.5}$ for $q < q_{\text{br}}$
Udalski et al. (2018)	7	–	$f(q) \propto q^{1.05_{-0.68}^{+0.78}}$	for $q < 10^{-4}$
Poleski et al. (2021)	5	3095	$f(s, q) = 1.04_{-0.57}^{+0.78} \times s^{1.09 \pm 0.64} \left(\frac{q}{1.7 \times 10^{-4}}\right)^{-1.15 \pm 0.25}$	only $2 < s < 6$
Koshimoto et al. (2021)	28	–	$f(R_L, M) \propto R_L^{0.2 \pm 0.4} M^{0.7_{-0.6}^{+0.8}}$	R_L is the Galactocentric lens distance

^a – number of planets detected; ^b – number of events analyzed; ^c – for definition of the planet occurrence rate, see Eq. 6.

Occurrence rates from high-magnification events

The planet occurrence rate can be derived either from a large number of events with a whole range of magnifications or from a much smaller number of high-magnification events. The peaks of high-magnification events are the most important because they give high chances of detecting planets, if the latter were present (Griest and Safizadeh 1998). The high-magnification events have two additional advantages: they are bright at the peak and can be selected a day or so before the peak. These features reduce the amount of telescope time needed to discover a planet. High-magnification events often get bright enough to be observed by a small-aperture telescopes and even amateur astronomers may collect scientifically useful photometry. Such an experiment was conducted by the Microlensing Follow Up Network (μFUN) and its results were presented by Gould et al. (2010). They analyzed data from a four-year-long experiment which densely followed-up 13 events with a peak magnification greater than 200. Six planets in five planetary events were detected in this experiment, which allowed the authors to measure the planet mass-ratio function:

$$f(s, q)|_{q=5 \times 10^{-3}} = 0.36 \pm 0.15 \text{ dex}^{-2}. \quad (9)$$

A larger sample of events was studied in a similar manner by Cassan et al. (2012). They used photometry collected by the Probing Lensing Anomalies Network (PLANET) collaboration. The planet detection efficiency was calculated for the (s, q) parameters and scaled to (a_{\perp}, m_p) . This scaling was done separately for each event based on the Einstein timescale (t_E) measured. Then, the projected sep-

aration a_{\perp} was further scaled to the semi-major axis a assuming isotropic circular orbits (Kubas et al. 2008). The PLANET collaboration detected three planets and used earlier studies (Sumi et al. 2010; Gould et al. 2010) as additional constraints. The result of the Cassan et al. (2012) investigation was:

$$f(a, m_p) = 10^{-0.62 \pm 0.22} \left(\frac{m_p}{M_{\text{Sat}}} \right)^{-0.73 \pm 0.17}, \quad (10)$$

where $M_{\text{Sat}} = 95 M_{\oplus}$ is the mass of Saturn. This planet occurrence rate was integrated over the semi-major axis range $0.5 \div 10$ au for Jupiter-mass ($0.3 \div 10 M_J$), cool Neptunes ($10 \div 30 M_{\oplus}$), and super-Earth planets ($5 \div 10 M_{\oplus}$) resulting in $17_{-9}^{+6}\%$, $52_{-29}^{+22}\%$, and $62_{-37}^{+32}\%$, respectively. These numbers indicated that planets frequently orbit stars in the Milky Way.

The results obtained by Cassan et al. (2012) were assumed as a baseline for the predictions of the planet yield by Penny et al. (2019) in their preparation of the microlensing survey for the *Nancy Grace Roman Space Telescope* (formerly *WFIRST*). The *Roman* telescope is currently predicted to be launched in 2026 or 2027, hence, it is likely that the Cassan et al. (2012) result will remain a reference for detailed preparations of the *Roman* microlensing observations and studies of results of these observations.

The above studies of microlensing planet occurrence rate were followed-up by studies that aimed at more detailed understanding of the whole population of planets. A joint analysis of microlensing and radial velocity results was conducted by Clanton and Gaudi (2014a,b). They concluded that the statistical results from both methods agree in the part of parameter space where their sensitivity overlaps. Furthermore, a single planetary occurrence rate was found consistent with constraints from microlensing, radial velocity, and direct imaging techniques (Clanton and Gaudi 2016).

Occurrence rates from modern microlensing surveys

The most detailed study of bound microlensing planet statistics was done based on the MOA survey data and presented by Suzuki et al. (2016). They used data collected between 2007 and 2012: 1474 events with 23 planets detected. These are planets detected from the MOA data alone. For each of these planets, the parameters used in the statistical analysis were taken from the fit to the light curve that combines all survey and follow-up data available. To analyze the occurrence rate, Suzuki et al. (2016) first plotted the histogram of $q_i/S(q_i)$, i.e., the number of detected planets corrected for survey sensitivity, where $S(q) = \int S(s, q) ds$. This histogram has a constant bin width in $\log q$ and an approximately constant slope for $\log q > -4.5$. There is no planet with a lower q . The shape of the histogram combined with a power-law shape of $S(q)$ points to a planet occurrence rate that is a broken power law of q , i.e.,

$$f(s, q; A, q_{\text{br}}, n, p, m) = \begin{cases} A \left(\frac{q}{q_{\text{br}}}\right)^n s^m & \text{for } q \geq q_{\text{br}} \\ A \left(\frac{q}{q_{\text{br}}}\right)^p s^m & \text{for } q < q_{\text{br}}. \end{cases} \quad (11)$$

This broken power-law is favored over the unbroken power-law by a Bayes factor of at least 21. The parameters of $f(s, q)$ were derived by jointly analyzing the MOA data with Gould et al. (2010) and Cassan et al. (2012) data. The final results are provided for an assumed fixed mass-ratio break at $q_{\text{br}} = 1.7 \times 10^{-4}$. We do not see a clear argument for fixing q_{br} at this value, and if the parameter is left free in the fits, then the uncertainty of p (i.e., the power-law exponent of q below the break) is larger than presented in Table 1.

Suzuki et al. (2016) calculated the planet occurrence rate as a function of microlensing parameters s and q . Translating it to the physical parameters (separation and mass) requires high-resolution imaging observations. Such observations have been collected for many events from the Suzuki et al. (2016) sample, for example as a part of the NASA Keck Key Strategic Mission Support program (e.g., Bhattacharya et al. 2018).

The results obtained by Suzuki et al. (2016) were compared with the predictions of the core-accretion theory of planet formation by Suzuki et al. (2018). They simulated a population of planets around lenses in all 1474 events studied by Suzuki et al. (2016); planets were simulated using approaches of two groups preparing such models: Ida and Lin (2004) and the Bern group (Mordasini et al. 2009). The agreement between the simulated and observed populations could not be found, even though a few different assumptions were used. The discrepancies between simulated and observed populations seem most problematic for $q \approx 2 \times 10^{-4}$. For a typical lens mass, this mass ratio corresponds to the mass range of failed gas giant cores, i.e., $\approx 20 \div 80 M_{\oplus}$. The core-accretion model predicts that there should be very few failed gas giant cores, which is contradicted by the microlensing findings. Additionally, Suzuki et al. (2018) point that the event OGLE-2012-BLG-0950 has the lens mass of $0.58 \pm 0.04 M_{\odot}$ and the planet mass of $39 \pm 8 M_{\oplus}$ (Bhattacharya et al. 2018), which is the kind of system that should be very rare.

The Suzuki et al. (2016) analysis was followed-up by more detailed studies. Udalski et al. (2018) studied the mass-ratio function for planets with $q < 10^{-4}$ based on all known such planets at that time, i.e., without limiting to planets found by a single survey. These planets were found using different observing approaches, which prevents using statistical methods typically used to derive the planet occurrence rate. Instead, Udalski et al. (2018) used a method called V'/V'_{max} , which was originally developed for studies of a luminosity function of quasars (Schmidt 1968). In this method, one assumes the ratio of a volume density of quasars at redshift z' and now $\rho(z')$ and calculates a generalized volume to each quasar detected at redshift z : $V'(z) = \int_0^z \rho(z') dV(z')$. For each quasar, one also calculates the generalized volume to the maximum redshift at which a given quasar could be discovered (V'_{max}). The functional form of $\rho(z)$ can be found by requesting that V'/V'_{max} values are consistent with being drawn from a uniform distribution from 0 to 1 (i.e., the mean should be 1/2, etc.). This method was used by Udalski et al. (2018) with $\rho(z)$ replaced by

$f(s, q)$ and $V(z)$ replaced by $S(q)$ and resulted in $f(q) \propto q^{1.05^{+0.78}_{-0.68}}$ based on seven planets with $q < 10^{-4}$.

The sample of 15 planets with $q < 3 \times 10^{-4}$ out of 16 such planets known at a time was analyzed by Jung et al. (2019). They noticed that the observed distribution of mass ratios is uniform in $\log q$. Since the sensitivity to planets decreases for smaller mass ratios, this observation indicated that the intrinsic frequency of planets above the putative break must increase for smaller q . Jung et al. (2019) additionally made a crucial assumption that the sensitivity to planets $S(q)$ as a function of q can be approximated as a simple power-law function, even below the putative break. Under that assumption, the observed distribution of $\log q$ depends on the location q_{br} and the “strength” of the mass-ratio break (that is, the change of the power-law slope). Jung et al. (2019) found that the sample of events they analyzed was consistent with the break at $q_{\text{br}} \approx 0.55 \times 10^{-4}$, much lower than assumed by Suzuki et al. (2016). Moreover, the change of the power-law slope at the break seemed to be considerable, $\Delta n > 3.3$, indicating a substantial drop in the number of low-mass planets.

Since the location of the break inferred by Jung et al. (2019) was close to the lowest- q planet in their sample, this immediately raised the possibility that the break may be an artifact of a sudden drop in sensitivity, not the paucity of low-mass planets, contrary to the assumption made by Jung et al. (2019). To check this hypothesis, a larger sample of uniformly selected planets was needed. This sample is currently being built with the KMTNet’s ANOMALYFINDER algorithm (Zang et al. 2021), which is responsible for the rapid growth in the number of discovered planets seen in Fig. 1. The application of the ANOMALYFINDER algorithm to the KMTNet data collected in 2016–2019 led to the discovery of about 100 exoplanets (Hwang et al. 2022; Wang et al. 2022; Zang et al. 2022, 2023; Gould et al. 2022a; Jung et al. 2022, 2023; Shin et al. 2023; Ryu et al. 2023), a statistical sample that is nearly an order of magnitude larger than that analyzed by Suzuki et al. (2016). That sample includes several planetary events with mass ratios smaller than $q = 5 \times 10^{-5}$, including OGLE-2019-BLG-1053 ($q = (1.25 \pm 0.13) \times 10^{-5}$; Zang et al. 2021), OGLE-2019-BLG-0960 ($q = (1.2 \div 1.6) \times 10^{-5}$; Yee et al. 2021), and KMT-2018-BLG-0029 ($q = (1.81 \pm 0.20) \times 10^{-5}$; Gould et al. 2020). Although the statistical analysis of the ANOMALYFINDER sample is still ongoing and its results were not published at the time of writing this review, we are certain that it will provide strong constraints on the shape of the low-mass planets mass-ratio function.

Galactic distribution of exoplanets

A sample of planetary microlensing events can be used to check how the frequency of planets changes with the position in the Galaxy. Such an investigation was first conducted by Penny et al. (2016) who found that planets in the Galactic bulge seem to be less common than in the Galactic disk. However, this result is very sensitive to a small number of π_{E} measurements (Penny et al. 2016), some of which are sus-

ceptible to systematic uncertainties. The planet occurrence rate as a function of the Galactocentric distance was studied by Koshimoto et al. (2021) but the dependence turned out to be statistically insignificant. One can compare the planet occurrence rate between Galactic disk and bulge, or in more general position in the Galaxy, using microlensing parallaxes measured from the comparison of the ground-based and satellite-based light curves (Zhu et al. 2017). Such satellite observations were already collected by the *Spitzer* satellite for a large number of events that were selected using well-defined criteria (Yee et al. 2015). The full analysis of these data has not yet been presented.

Occurrence Rates of Free-floating Planets

Gravitational microlensing can be also employed to search for and study an elusive population of free-floating planets. These objects, sometimes referred to as rogue planets or unbound planets, are thought to be inevitable outcomes of planet formation processes. There is no universally agreed definition of free-floating planets: For the purpose of this chapter, any object with a mass smaller than the deuterium-burning limit ($\approx 13 M_J$, where M_J is the mass of Jupiter) that is not gravitationally bound to a more massive celestial body is called a free-floating planet.

Various processes can lead to the formation of free-floating planets. Such objects may form via gravitational collapse, in a similar way as stars (e.g., Padoan and Nordlund 2002; Hennebelle and Chabrier 2008), or as failed stellar embryos (e.g., Reipurth and Clarke 2001; Whitworth and Zinnecker 2004). If they are massive ($\gtrsim 4 \div 5 M_J$), nearby, and young (at most several Myr) enough, they can be directly detected. Indeed, many planetary-mass objects and objects on a boundary between planets and brown dwarfs were discovered in nearby star-forming regions (e.g., Peña Ramírez et al. 2012; Scholz et al. 2012), young associations (e.g., Gagné et al. 2017; Lodieu et al. 2021; Miret-Roig et al. 2022), as well as in the solar neighborhood (e.g., Kirkpatrick et al. 2019, 2021).

Free-floating planets may also have formed in protoplanetary disks, in a way similar to that in which ordinary extrasolar planets form, either by core accretion (Pollack et al. 1996) or disk instability (Boss 1998), and subsequently ejected from their parent planetary systems. Various processes may be responsible for the ejections. The planet–planet scattering (e.g., Rasio and Ford 1996; Weidenschilling and Marzari 1996; Lin and Ida 1997; Chatterjee et al. 2008) is the most likely one. At least 75% of systems with giant planets (if not 90–95%) should have experienced the planet–planet scattering in the past (according to Raymond and Morbidelli 2022, and references therein), in order to explain the observed distribution of eccentricities of giant planets. These dynamical interactions are likely to disrupt the orbits of inner terrestrial planets or planetary embryos and ultimately lead to their ejection (Veras and Armitage 2005; Matsumura et al. 2013; Carrera et al. 2016; Matsumoto et al. 2020), as demonstrated in extensive simulations by Pfyffer et al. (2015), Ma et al. (2016), or Barclay et al. (2017), among others. Other mechanisms capable of

ejecting planets from their parent systems include dynamical interactions in binary and multiple star systems (e.g., Kaib et al. 2013; Sutherland and Fabrycky 2016), interactions in stellar clusters and star-forming regions (e.g., Spurzem et al. 2009; Parker and Quanz 2012; van Elteren et al. 2019; Daffern-Powell et al. 2022; Rickman et al. 2023), interactions in gravitationally unstable protoplanetary disks (Boss 2023), stellar fly-bys (e.g., Malmberg et al. 2011; Bailey and Fabrycky 2019), or the effects of the post-main-sequence evolution of the host star (e.g., Veras et al. 2011). The ejected planets are expected to be predominantly of low-mass, rendering it virtually impossible to observe them directly.

Fortunately, free-floating planets, even the least massive ones, may be detected by means of their gravity, via gravitational microlensing. There are, however, two major factors that limit their detectability. First, the smaller the mass of the planet, the shorter the duration of the event. The Einstein timescale t_E of the microlensing event depends on its angular Einstein radius θ_E and the relative lens–source proper motion μ_{rel} :

$$t_E = \frac{\theta_E}{\mu_{\text{rel}}} = 0.11 \text{ d} \left(\frac{M}{1 M_{\oplus}} \right)^{1/2} \left(\frac{\pi_{\text{rel}}}{0.1 \text{ mas}} \right)^{1/2} \left(\frac{\mu_{\text{rel}}}{5 \text{ mas yr}^{-1}} \right)^{-1}, \quad (12)$$

where M is the mass of the planet and π_{rel} is the relative lens–source parallax. Microlensing events by Jupiter-mass objects have timescales on the order of $1 \div 2$ d, whereas those by terrestrial-mass planets have timescales of only a few hours. Thus, detecting free-floating planets with microlensing requires high-cadence observations (at least one observation per hour).

Another factor that limits the detectability of free-floating planets is the finite-source effect. This effect is observed when the angular radius of the star being lensed θ_* becomes comparable to the angular Einstein radius. For typical values of free-floating planets, the Eq. 5 becomes:

$$\rho = 0.4 \left(\frac{\theta_*}{0.6 \mu\text{as}} \right) \left(\frac{M}{1 M_{\oplus}} \right)^{-1/2} \left(\frac{\pi_{\text{rel}}}{0.1 \text{ mas}} \right)^{-1/2}, \quad (13)$$

where $0.6 \mu\text{as}$ is the angular radius of a $1 R_{\odot}$ star located in the Galactic center distance. If $\rho \gg 1$, the magnification of the event quickly falls as $A = 1 + 2/\rho^2$. Therefore, the least massive planets produce microlensing signals of a low amplitude, whose light curve shape may resemble that of an “inverted” planetary transit. On a positive note, the detection of finite-source effects in the light curve of the event allows us to directly determine the angular Einstein radius of the planet, which further constrains the lens mass.

The first claims about a possible population of free-floating planets did not last long. Sahu et al. (2001) observed stars behind the globular cluster M22 with the *Hubble Space Telescope* and found six extremely short, unresolved “events” (lasting less than 6 min each). However, it was quickly realized that these were artifacts caused by cosmic ray hits rather than genuine astrophysical sources (Sahu et al. 2002).

Another attempt to study the population of free-floating planets in the Milky Way was made by Sumi et al. (2011), who analyzed the light curves of 474 microlensing events detected by the MOA survey during the years 2006–2007. The MOA group was the first to conduct a microlensing survey of the Galactic bulge with a high cadence ($10 \div 50$ min), hence, MOA observations were sensitive to the shortest-timescale events. Sumi et al. (2011) found an apparent excess of short-timescale events ($t_E = 0.5 \div 2$ d), which they claimed was due to a population of about two Jupiter-mass free-floating planets per star. Over a decade later, however, these observations turned out to be severely affected by systematic errors due to differential refraction (Koshimoto et al. 2023). Nevertheless, the work by Sumi et al. (2011) sparked many theoretical studies on the origin of free-floating planets and opened up the new field.

The claims by Sumi et al. (2011) were met with some skepticism in the community, partly because it was difficult to explain how such a large population of Jupiter-mass free-floaters could have formed (e.g., Veras and Raymond 2012), and partly because the infrared surveys of young clusters and star-forming regions did not find that many planetary-mass objects (e.g., Peña Ramírez et al. 2012; Scholz et al. 2012). The start of the fourth phase of the OGLE survey in 2010 (Udalski et al. 2015) raised hopes for an independent evaluation of the population of free-floating planets. OGLE observed about 50 million stars in an area greater than 12 deg^2 at a high cadence ($20 \div 60$ min).

The results of a nearly six-year-long observing campaign by the OGLE survey were reported by Mróz et al. (2017), who analyzed the light curves of 2617 microlensing events detected during the years 2010–2015, and measured the distribution of their Einstein timescales. Mróz et al. (2017) did not find significant excess of events with timescales $t_E = 1 \div 2$ d, placing a 95% upper limit on the frequency of Jupiter-mass free-floating planets of 0.25 planets per main-sequence star. Moreover, they detected six events with extremely short timescales, $t_E = 0.1 \div 0.5$ d, which were indicative of a population of Earth-mass and super-Earth-mass free-floating planets, as predicted by planet-formation theories. The distribution of Einstein timescales of events detected by Mróz et al. (2017) (corrected for selection biases) is shown in the left panel of Fig. 3.

The discovery of this new population of low-mass free-floating planet candidates coincided with the start of the KMTNet survey (Kim et al. 2016). By combining data from OGLE and KMTNet, Mróz et al. (2018) detected OGLE-2016-BLG-1540, the first short-timescale ($t_E = 0.320 \pm 0.003$ d) event exhibiting finite-source effects, which enabled the authors to measure its angular Einstein radius. This discovery was soon followed by the detection of a handful of events exhibiting finite-source effects by OGLE, KMTNet, and other surveys (Mróz et al. 2019, 2020a,b; Ryu et al. 2021; Kim et al. 2021; Koshimoto et al. 2023), including likely terrestrial-mass planets (Mróz et al. 2020a; Koshimoto et al. 2023). These detections greatly strengthened the conclusions of Mróz et al. (2017), as they proved the existence of a population of microlensing events with small angular Einstein radii ($\lesssim 10 \mu\text{as}$) and short timescales ($t_E \lesssim 0.5$ d).

The measurements of the angular Einstein radii are particularly important because, unlike Einstein timescales, they do not depend on the relative lens–source proper motion. In particular, Kim et al. (2021) and Ryu et al. (2021) noticed that angular Einstein radii of free-floating planet candidates are separated by a gap ($10\mu\text{as} \lesssim \theta_E \lesssim 30\mu\text{as}$), dubbed the “Einstein desert”, from those of brown dwarfs and stars (see the right panel of Fig. 3). A similar gap is seen in the distribution of Einstein timescales measured by Mróz et al. (2017).

The Einstein desert was a subject of a detailed investigation by Gould et al. (2022b), who systematically analyzed giant-source events exhibiting finite-source effects in the 2016–2019 KMTNet microlensing data set. Thanks to this systematic approach to searches for events with finite-source effects, Gould et al. (2022b) estimated a simple functional form of the detection efficiency as a function of θ_E (in good agreement with that calculated with extensive simulations carried out by Sumi et al. (2023)). Gould et al. (2022b) demonstrated that the distribution of angular Einstein radii of events observed by KMTNet is consistent with a power law distribution of masses of free-floating planet candidates: $dN/d\log M = (0.4 \pm 0.2)(M/38M_\oplus)^{-p}/\text{star}$, with $0.9 \lesssim p \lesssim 1.2$. The power-law index $p < 0.9$ would be inconsistent with the Einstein desert, while $p > 1.2$ would be allowed by the data, but it was deemed improbable based on physical arguments.

The power-law mass function of free-floating planet candidates was confirmed by the analysis of a statistical sample of about 3500 microlensing events detected by the MOA survey in 2006–2014 (Koshimoto et al. 2023; Sumi et al. 2023). They were the first to calculate the event detection efficiency as a function of both t_E and θ_E . A detailed statistical analysis of the MOA data set enabled Sumi et al. (2023) to measure the mass function of free-floating planet candidates $dN/d\log M = (0.49^{+0.12}_{-0.32})(M/38M_\oplus)^{-p}/\text{star}$, with $p = 0.94^{+0.47}_{-0.27}$, in remarkable agreement with that found by Gould et al. (2022b). The Sumi et al. (2023) mass function extends down to masses of just $0.33M_\oplus$, but its shape at such low masses is poorly constrained because there is only a single detection in this mass regime.

A general picture of the population of free-floating planet candidates emerges from the three major studies discussed (Mróz et al. 2017; Gould et al. 2022b; Sumi et al. 2023). These studies are all based on independent data sets and independent data analysis methods, yet they converge to the same conclusion that the mass function of free-floating planet candidates can be approximated by a power law with the index $p \approx 1$ and predict about $\sim 7^{+7}_{-5}$ free-floaters more massive than $1M_\oplus$ per star. The number of lower-mass objects is even greater, it approximately scales as $(M_{\min}/1M_\oplus)^p$, where M_{\min} is the minimal mass of free-floating planets considered. Gould et al. (2022b) considered planets more massive than $\approx 1M_\oplus$, whereas the study of Sumi et al. (2023) was sensitive to even less massive objects ($\gtrsim 0.3M_\oplus$). The results of all three studies (Mróz et al. 2017; Gould et al. 2022b; Sumi et al. 2023) seem to indicate that the number of free-floating planet candidates is of the same order (or even greater) than the number of gravitationally bound planets. If confirmed, this would indicate that ejections may play a major role during the planet formation and shape the mass function of bound exoplanets.

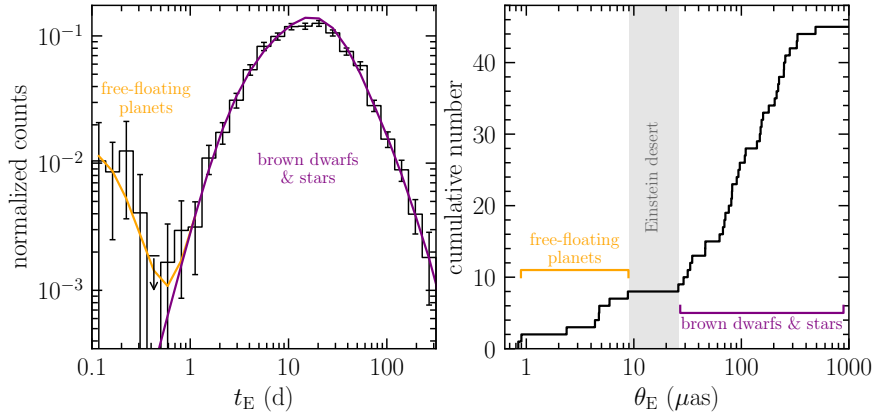


Fig. 3 Both the distribution of Einstein timescales (left) and angular Einstein radii (right) of single-lens microlensing events indicate the presence of two populations of objects: free-floating planet candidates, and brown dwarfs and stars. These populations are separated by the so-called Einstein desert. Data were taken from Mróz et al. (2017, 2019, 2020a); Ryu et al. (2021); Gould et al. (2022b); Koshimoto et al. (2023).

All these studies, however, suffer from the same caveat. Light curves of short-timescale microlensing events detected in the OGLE, KMTNet, and MOA data are consistent with those by isolated objects. However, it cannot be ruled out that all (or some) detected planets may have a widely separated stellar companion. If the host star were located sufficiently far from the lensing object (the planet), it would not leave any detectable signatures in the light curve of the event, rendering it difficult to distinguish between a free-floating and a wide-orbit planet scenario (e.g., Han and Kang 2003; Han et al. 2005). The available photometric data enable us to rule out the presence of a putative host star within only approximately five Einstein radii (projected separation of ≈ 12 au) of the planet (e.g., Mróz et al. 2018; Kim et al. 2021). We note that the widest separation low-mass microlensing planet has $s = 5.25$ (Poleski et al. 2014). It is thus possible that some (or even all) of the detected objects are actually orbiting a distant host star in a wide orbit. For example, the distribution of the smallest θ_E events found by Gould et al. (2022b) was considered consistent with being fully caused by the wide-orbit planet distribution derived by Poleski et al. (2021). Adaptive optics observations of free-floating planet candidates ruled out some possible host stars (Mróz et al. 2023). However, deeper imaging observations are needed to distinguish between the free-floating planet and wide-orbit planet hypotheses, such observations will be possible with the *JWST* or the next generation of large 30-m-class ground-based telescopes (e.g., Gould 2016a).

There is no doubt that the population of low-mass free-floating planet candidates that were uncovered by ground-based surveys will be subject to more detailed investigations in the future. The planned space-based microlensing experiments are especially promising because they enable almost continuous coverage of light curves, and the exquisite space-based photometry allows one to detect low-amplitude events

(e.g., Henderson and Shvartzvald 2016). The first attempt to carry out a space-based microlensing survey was the Campaign 9 of the *K2* mission (*Kepler* satellite), which observed an area of 3.7 deg^2 toward the Galactic bulge from 2016 April 22 through July 2 (Henderson et al. 2016). These observations were obtained before Mróz et al. (2017) results were published, hence, the experiment was planned based on Sumi et al. (2011) free-floating planet rate. The *Kepler* spacecraft was not designed to observe dense Galactic bulge fields. Nevertheless, McDonald et al. (2021) detected four candidates for short-duration microlensing events. Their origin remains unknown, unfortunately, because McDonald et al. (2021) were able to measure only the effective timescale, $t_{\text{eff}} = t_E u_0$, which is a combination of the Einstein timescale and the impact parameter of the event.

The *Roman* telescope is planned to carry out a time-domain near-infrared survey of the Galactic bulge in the late 2020s and early 2030s (Penny et al. 2019). *Roman* is designed to observe the Galactic bulge during six 72-d-long seasons. Equipped with a 2.4 m mirror and HAWAII HgCdTe detectors with a field of view of 0.282 deg^2 , *Roman* is predicted to detect $\approx 27,000$ microlensing events in total (Penny et al. 2019). Johnson et al. (2020) estimated that *Roman* may detect at least 250 free-floating planets with masses down to that of Mars, assuming their mass function is identical to that of bound planets (Cassan et al. 2012). Assuming the mass function of Sumi et al. (2023), *Roman* is expected to detect 988^{+1848}_{-566} free-floating planets. Similarly, the *Earth 2.0 (ET)* mission by the Chinese Academy of Sciences is a proposed space-based telescope designed to carry out transit and microlensing surveys (Ge et al. 2022), following the arguments put forward by Gould et al. (2021). Its planned launch date is 2027. The *ET* mission will consist of seven 30-cm-class telescopes, one of which is planned to be dedicated to microlensing observations. The microlensing telescope is designed to have the same field of view (4 deg^2) and pixel scale ($0.4''$) as the KMTNet telescopes. The *ET* mission is predicted to detect about 600 free-floating planets assuming the mass function of Gould et al. (2022b) and the duration of the survey of 4 yr.

The planned space-based missions make also promise for direct measurements of the masses of free-floating planet candidates, which is possible owing to the satellite microlensing parallax effects (the same event simultaneously observed from the ground and a sufficiently separated space-based observatory should look differently). Events detected by the *Roman* or the *Earth 2.0* missions may be additionally observed with ground-based (Zhu and Gould 2016; Street et al. 2018; Gould et al. 2021) and space-based facilities: *Euclid* (Bachelet and Penny 2019; Ban 2020; Bachelet et al. 2022), *Chinese Space Station Telescope* (Yan and Zhu 2022), or *CLEOPATRA* (Barry et al. 2022). These additional observations will enable us to better understand the population of free-floating planets and the processes that occur at the early stages of planet formation.

Cross-References

- Finding Planets via Gravitational Microlensing
- Microlensing Surveys for Exoplanet Research (OGLE Survey Perspective)
- Microlensing Surveys for Exoplanet Research (MOA)
- Korea Microlensing Telescope Network

Acknowledgements We thank Andrzej Udalski, Weicheng Zang, and Aparna Bhattacharya for their comments on the early draft of the manuscript. This research has made use of the NASA Exoplanet Archive, which is operated by the California Institute of Technology, under contract with the National Aeronautics and Space Administration under the Exoplanet Exploration Program. Work by RP was supported by the Polish National Agency for Academic Exchange grant “Polish Returns 2019.”

References

- Alcock C, Allsman RA, Alves DR et al. (2001) Direct detection of a microlens in the Milky Way. *Nature*414(6864):617–619
- Bachelet E Penny M (2019) WFIRST and EUCLID: Enabling the Microlensing Parallax Measurement from Space. *ApJ*880(2):L32
- Bachelet E, Specht D, Penny M et al. (2022) Euclid-Roman joint microlensing survey: Early mass measurement, free floating planets, and exomoons. *A&A*664:A136
- Bailey N Fabrycky D (2019) Stellar Flybys Interrupting Planet-Planet Scattering Generates Oort Planets. *AJ*158(2):94
- Ban M (2020) Probability of simultaneous parallax detection for free-floating planet microlensing events near Galactic Centre. *MNRAS*494(3):3235–3252
- Barclay T, Quintana EV, Raymond SN Penny MT (2017) The Demographics of Rocky Free-floating Planets and their Detectability by WFIRST. *ApJ*841(2):86
- Barry RK, Olmschenk G, Ravizza F et al. (2022) CLEoPATRA: contemporaneous lensing parallax and autonomous transient assay. In: Coyle LE, Matsuura S Perrin MD (eds) *Space Telescopes and Instrumentation 2022: Optical, Infrared, and Millimeter Wave*, Society of Photo-Optical Instrumentation Engineers (SPIE) Conference Series, vol 12180, p 121800D, DOI 10.1117/12.2620310
- Batista V (2018) Finding planets via gravitational microlensing. In: Deeg HJ Belmonte JA (eds) *Handbook of Exoplanets*, Springer International Publishing, Cham, pp 659–687, DOI 10.1007/978-3-319-55333-7_120
- Batista V, Beaulieu JP, Bennett DP et al. (2015) Confirmation of the OGLE-2005-BLG-169 Planet Signature and Its Characteristics with Lens-Source Proper Motion Detection. *ApJ*808(2):170
- Bennett DP, Bhattacharya A, Anderson J et al. (2015) Confirmation of the Planetary Microlensing Signal and Star and Planet Mass Determinations for Event OGLE-2005-BLG-169. *ApJ*808(2):169
- Bhattacharya A, Beaulieu JP, Bennett DP et al. (2018) WFIRST Exoplanet Mass-measurement Method Finds a Planetary Mass of $39 \pm 8 M_{\oplus}$ for OGLE-2012-BLG-0950Lb. *AJ*156(6):289
- Boss AP (1998) Evolution of the Solar Nebula. IV. Giant Gaseous Protoplanet Formation. *ApJ*503(2):923–937
- Boss AP (2023) Orbital Migration of Protoplanets in a Marginally Gravitationally Unstable Disk. II. Migration, Merging, and Ejection. *ApJ*943(2):101
- Carrera D, Davies MB Johansen A (2016) Survival of habitable planets in unstable planetary systems. *MNRAS*463(3):3226–3238

- Cassan A, Kubas D, Beaulieu JP et al. (2012) One or more bound planets per Milky Way star from microlensing observations. *Nature* 481(7380):167–169
- Chatterjee S, Ford EB, Matsumura S, Rasio FA (2008) Dynamical Outcomes of Planet-Planet Scattering. *ApJ* 686(1):580–602
- Clanton C, Gaudi BS (2014a) Synthesizing Exoplanet Demographics from Radial Velocity and Microlensing Surveys. I. Methodology. *ApJ* 791(2):90
- Clanton C, Gaudi BS (2014b) Synthesizing Exoplanet Demographics from Radial Velocity and Microlensing Surveys. II. The Frequency of Planets Orbiting M Dwarfs. *ApJ* 791(2):91
- Clanton C, Gaudi BS (2016) Synthesizing Exoplanet Demographics: A Single Population of Long-period Planetary Companions to M Dwarfs Consistent with Microlensing, Radial Velocity, and Direct Imaging Surveys. *ApJ* 819(2):125
- Daffern-Powell EC, Parker RJ, Quanz SP (2022) The Great Planetary Heist: theft and capture in star-forming regions. *MNRAS* 514(1):920–934
- Fukui A, Suzuki D, Koshimoto N et al. (2019) Kojima-1Lb Is a Mildly Cold Neptune around the Brightest Microlensing Host Star. *AJ* 158(5):206
- Gagné J, Faherty JK, Mamajek EE et al. (2017) BANYAN. IX. The Initial Mass Function and Planetary-mass Object Space Density of the TW HYA Association. *ApJS* 228(2):18
- Gaudi BS (2012) Microlensing Surveys for Exoplanets. *ARA&A* 50:411–453
- Gaudi BS, Sackett PD (2000) Detection Efficiencies of Microlensing Data Sets to Stellar and Planetary Companions. *ApJ* 528(1):56–73
- Gaudi BS, Albrow MD, An J et al. (2002) Microlensing Constraints on the Frequency of Jupiter-Mass Companions: Analysis of 5 Years of PLANET Photometry. *ApJ* 566(1):463–499
- Ge J, Zhang H, Zang W et al. (2022) ET White Paper: To Find the First Earth 2.0. arXiv e-prints arXiv:2206.06693
- Gould A (1992) Extending the MACHO Search to approximately 10.6 M sub sun. *ApJ* 392:442
- Gould A (1994) Proper Motions of MACHOs. *ApJ* 421:L71
- Gould A (2016a) Microlensing by Kuiper, Oort, and Free-Floating Planets. *Journal of Korean Astronomical Society* 49(4):123–126
- Gould A (2016b) Microlensing Planets. In: Bozza V, Mancini L, Sozzetti A (eds) *Methods of Detecting Exoplanets: 1st Advanced School on Exoplanetary Science, Astrophysics and Space Science Library*, vol 428, p 135, DOI 10.1007/978-3-319-27458-4_3
- Gould A, Loeb A (1992) Discovering Planetary Systems through Gravitational Microlenses. *ApJ* 396:104
- Gould A, Dong S, Gaudi BS et al. (2010) Frequency of Solar-like Systems and of Ice and Gas Giants Beyond the Snow Line from High-magnification Microlensing Events in 2005–2008. *ApJ* 720(2):1073–1089
- Gould A, Ryu YH, Calchi Novati S et al. (2020) KMT-2018-BLG-0029Lb: A Very Low Mass-Ratio Spitzer Microlens Planet. *Journal of Korean Astronomical Society* 53:9–26
- Gould A, Zang WC, Mao S, Dong SB (2021) Masses for free-floating planets and dwarf planets. *Research in Astronomy and Astrophysics* 21(6):133
- Gould A, Han C, Zang W et al. (2022a) Systematic KMTNet planetary anomaly search. V. Complete sample of 2018 prime-field. *A&A* 664:A13
- Gould A, Jung YK, Hwang KH et al. (2022b) Free-Floating Planets, the Einstein Desert, and 'OUMUAMUA. *Journal of Korean Astronomical Society* 55:173–194
- Griest K, Safizadeh N (1998) The Use of High-Magnification Microlensing Events in Discovering Extrasolar Planets. *ApJ* 500(1):37–50
- Han C, Kang YW (2003) Probing the Spatial Distribution of Extrasolar Planets with Gravitational Microlensing. *ApJ* 596(2):1320–1326
- Han C, Gaudi BS, An JH, Gould A (2005) Microlensing Detection and Characterization of Wide-Separation Planets. *ApJ* 618(2):962–972
- Henderson CB, Shvartzvald Y (2016) On the Feasibility of Characterizing Free-floating Planets with Current and Future Space-based Microlensing Surveys. *AJ* 152(4):96

- Henderson CB, Poleski R, Penny M et al. (2016) Campaign 9 of the K2 Mission: Observational Parameters, Scientific Drivers, and Community Involvement for a Simultaneous Space- and Ground-based Microlensing Survey. *PASP*128(970):124,401
- Hennebelle P Chabrier G (2008) Analytical Theory for the Initial Mass Function: CO Clumps and Prestellar Cores. *ApJ*684(1):395–410
- Hwang KH, Zang W, Gould A et al. (2022) Systematic KMTNet Planetary Anomaly Search. II. Six New $q < 2 \times 10^{-4}$ Mass-ratio Planets. *AJ*163(2):43
- Ida S Lin DNC (2004) Toward a Deterministic Model of Planetary Formation. I. A Desert in the Mass and Semimajor Axis Distributions of Extrasolar Planets. *ApJ*604(1):388–413
- Johnson SA, Penny M, Gaudi BS et al. (2020) Predictions of the Nancy Grace Roman Space Telescope Galactic Exoplanet Survey. II. Free-floating Planet Detection Rates. *AJ*160(3):123
- Jung YK, Gould A, Zang W et al. (2019) KMT-2017-BLG-0165Lb: A Super-Neptune-mass Planet Orbiting a Sun-like Host Star. *AJ*157(2):72
- Jung YK, Zang W, Han C et al. (2022) Systematic KMTNet Planetary Anomaly Search. VI. Complete Sample of 2018 Sub-prime-field Planets. *AJ*164(6):262
- Jung YK, Zang W, Wang H et al. (2023) Systematic KMTNet Planetary Anomaly Search. VIII. Complete Sample of 2019 Subprime Field Planets. *AJ*165(6):226
- Kaib NA, Raymond SN Duncan M (2013) Planetary system disruption by Galactic perturbations to wide binary stars. *Nature*493(7432):381–384
- Kim HW, Hwang KH, Gould A et al. (2021) KMT-2019-BLG-2073: Fourth Free-floating Planet Candidate with $\theta_E < 10 \mu\text{as}$. *AJ*162(1):15
- Kim SL, Lee CU, Park BG et al. (2016) KMTNET: A Network of 1.6 m Wide-Field Optical Telescopes Installed at Three Southern Observatories. *Journal of Korean Astronomical Society* 49(1):37–44
- Kirkpatrick JD, Martin EC, Smart RL et al. (2019) Preliminary Trigonometric Parallaxes of 184 Late-T and Y Dwarfs and an Analysis of the Field Substellar Mass Function into the “Planetary” Mass Regime. *ApJS*240(2):19
- Kirkpatrick JD, Gelino CR, Faherty JK et al. (2021) The Field Substellar Mass Function Based on the Full-sky 20 pc Census of 525 L, T, and Y Dwarfs. *ApJS*253(1):7
- Koshimoto N, Bennett DP, Suzuki D Bond IA (2021) No Large Dependence of Planet Frequency on Galactocentric Distance. *ApJ*918(1):L8
- Koshimoto N, Sumi T, Bennett DP et al. (2023) Terrestrial- and Neptune-mass Free-Floating Planet Candidates from the MOA-II 9 yr Galactic Bulge Survey. *AJ*166(3):107
- Kubas D, Cassan A, Dominik M et al. (2008) Limits on additional planetary companions to OGLE 2005-BLG-390L. *A&A*483(1):317–324
- Lin DNC Ida S (1997) On the Origin of Massive Eccentric Planets. *ApJ*477(2):781–791
- Lodieu N, Hambly NC Cross NJG (2021) Exploring the planetary-mass population in the Upper Scorpius association. *MNRAS*503(2):2265–2279
- Ma S, Mao S, Ida S, Zhu W Lin DNC (2016) Free-floating planets from core accretion theory: microlensing predictions. *MNRAS*461(1):L107–L111
- Madsen S Zhu W (2019) A Pair of Planets Likely in Mean-motion Resonance From Gravitational Microlensing. *ApJ*878(2):L29
- Malmberg D, Davies MB Hogg DC (2011) The effects of fly-bys on planetary systems. *MNRAS*411(2):859–877
- Mao S Paczyński B (1991) Gravitational Microlensing by Double Stars and Planetary Systems. *ApJ*374:L37
- Matsumoto Y, Gu PG, Kokubo E, Oshino S Omiya M (2020) Ejection of close-in super-Earths around low-mass stars in the giant impact stage. *A&A*642:A23
- Matsumura S, Ida S Nagasawa M (2013) Effects of Dynamical Evolution of Giant Planets on Survival of Terrestrial Planets. *ApJ*767(2):129
- McDonald I, Kerins E, Poleski R et al. (2021) Kepler K2 Campaign 9 - I. Candidate short-duration events from the first space-based survey for planetary microlensing. *MNRAS*505(4):5584–5602

- Medford MS, Abrams NS, Lu JR, Nugent P, Lam CY (2023) 60 Microlensing Events from the Three Years of Zwicky Transient Facility Phase One. *ApJ*947(1):24
- Mirret-Roig N, Bouy H, Raymond SN et al. (2022) A rich population of free-floating planets in the Upper Scorpius young stellar association. *Nature Astronomy* 6:89–97
- Mordasini C, Alibert Y, Benz W (2009) Extrasolar planet population synthesis. I. Method, formation tracks, and mass-distance distribution. *A&A*501(3):1139–1160
- Mróz P, Udalski A, Skowron J et al. (2017) No large population of unbound or wide-orbit Jupiter-mass planets. *Nature*548(7666):183–186
- Mróz P, Ryu YH, Skowron J et al. (2018) A Neptune-mass Free-floating Planet Candidate Discovered by Microlensing Surveys. *AJ*155(3):121
- Mróz P, Udalski A, Bennett DP et al. (2019) Two new free-floating or wide-orbit planets from microlensing. *A&A*622:A201
- Mróz P, Poleski R, Gould A et al. (2020a) A Terrestrial-mass Rogue Planet Candidate Detected in the Shortest-timescale Microlensing Event. *ApJ*903(1):L11
- Mróz P, Poleski R, Han C et al. (2020b) A Free-floating or Wide-orbit Planet in the Microlensing Event OGLE-2019-BLG-0551. *AJ*159(6):262
- Mróz P, Ban M, Marty P, Poleski R (2023) Free-floating or wide-orbit? Keck adaptive-optics observations reveal no host stars near free-floating planet candidates. *arXiv e-prints* arXiv:2303.04610
- Nemiroff RJ, Wickramasinghe WADT (1994) Finite Source Sizes and the Information Content of Macho-Type Lens Search Light Curves. *ApJ*424:L21
- Paczynski B (1986) Gravitational Microlensing by the Galactic Halo. *ApJ*304:1
- Padoan P, Nordlund Å (2002) The Stellar Initial Mass Function from Turbulent Fragmentation. *ApJ*576(2):870–879
- Parker RJ, Quanz SP (2012) The effects of dynamical interactions on planets in young substructured star clusters. *MNRAS*419(3):2448–2458
- Peña Ramírez K, Béjar VJS, Zapatero Osorio MR, Petr-Gotzens MG, Martín EL (2012) New Isolated Planetary-mass Objects and the Stellar and Substellar Mass Function of the σ Orionis Cluster. *ApJ*754(1):30
- Penny MT, Henderson CB, Clanton C (2016) Is the Galactic Bulge Devoid of Planets? *ApJ*830(2):150
- Penny MT, Gaudi BS, Kerins E et al. (2019) Predictions of the WFIRST Microlensing Survey. I. Bound Planet Detection Rates. *ApJS*241(1):3
- Pfytter S, Alibert Y, Benz W, Swoboda D (2015) Theoretical models of planetary system formation. II. Post-formation evolution. *A&A*579:A37
- Poleski R, Skowron J, Udalski A et al. (2014) Triple Microlens OGLE-2008-BLG-092L: Binary Stellar System with a Circumprimary Uranus-type Planet. *ApJ*795(1):42
- Poleski R, Skowron J, Mróz P et al. (2021) Wide-Orbit Exoplanets are Common. Analysis of Nearly 20 Years of OGLE Microlensing Survey Data. *Acta Astron*71(1):1–23
- Pollack JB, Hubickyj O, Bodenheimer P et al. (1996) Formation of the Giant Planets by Concurrent Accretion of Solids and Gas. *Icarus*124(1):62–85
- Rasio FA, Ford EB (1996) Dynamical instabilities and the formation of extrasolar planetary systems. *Science* 274:954–956
- Raymond SN, Morbidelli A (2022) Planet Formation: Key Mechanisms and Global Models. In: Biazzo K, Bozza V, Mancini L, Sozzetti A (eds) *Demographics of Exoplanetary Systems*, Lecture Notes of the 3rd Advanced School on Exoplanetary Science, Astrophysics and Space Science Library, vol 466, pp 3–82, DOI 10.1007/978-3-030-88124-5_1
- Reipurth B, Clarke C (2001) The Formation of Brown Dwarfs as Ejected Stellar Embryos. *AJ*122(1):432–439
- Rhie SH, Bennett DP, Becker AC et al. (2000) On Planetary Companions to the MACHO 98-BLG-35 Microlens Star. *ApJ*533(1):378–391
- Rickman H, Wajer P, Przyłuski R et al. (2023) Breakdown of planetary systems in embedded clusters. *MNRAS*520(1):637–648

- Rodriguez AC, Mróz P, Kulkarni SR et al. (2022) Microlensing Events in the Galactic Plane Using the Zwicky Transient Facility. *ApJ*927(2):150
- Ryu YH, Mróz P, Gould A et al. (2021) KMT-2017-BLG-2820 and the Nature of the Free-floating Planet Population. *AJ*161(3):126
- Ryu YH, Udalski A, Yee JC et al. (2023) Systematic KMTNet Planetary Anomaly Search. X. Complete Sample of 2017 Prime-Field Planets. arXiv e-prints arXiv:2307.13359
- Sahu KC, Casertano S, Livio M et al. (2001) Gravitational microlensing by low-mass objects in the globular cluster M22. *Nature*411(6841):1022–1024
- Sahu KC, Anderson J King IR (2002) A Reexamination of the “Planetary” Lensing Events in M22. *ApJ*565(1):L21–L24
- Schmidt M (1968) Space Distribution and Luminosity Functions of Quasi-Stellar Radio Sources. *ApJ*151:393
- Scholz A, Jayawardhana R, Muzic K et al. (2012) Substellar Objects in Nearby Young Clusters (SONYC). VI. The Planetary-mass Domain of NGC 1333. *ApJ*756(1):24
- Shin IG, Yee JC, Zang W et al. (2023) Systematic KMTNet Planetary Anomaly Search. IX. Complete Sample of 2016 Prime-field Planets. *AJ*166(3):104
- Shvartzvald Y, Mao D, Udalski A et al. (2016) The frequency of snowline-region planets from four years of OGLE-MOA-Wise second-generation microlensing. *MNRAS*457(4):4089–4113
- Skowron J, Udalski A, Gould A et al. (2011) Binary Microlensing Event OGLE-2009-BLG-020 Gives Verifiable Mass, Distance, and Orbit Predictions. *ApJ*738(1):87
- Snodgrass C, Horne K Tsapras Y (2004) The abundance of Galactic planets from OGLE-III 2002 microlensing data. *MNRAS*351(3):967–975
- Spurzem R, Giersz M, Heggie DC Lin DNC (2009) Dynamics of Planetary Systems in Star Clusters. *ApJ*697(1):458–482
- Street RA, Lund MB, Donachie M et al. (2018) Unique Science from a Coordinated LSST-WFIRST Survey of the Galactic Bulge. arXiv e-prints arXiv:1812.04445
- Sumi T, Abe F, Bond IA et al. (2003) Microlensing Optical Depth toward the Galactic Bulge from Microlensing Observations in Astrophysics Group Observations during 2000 with Difference Image Analysis. *ApJ*591(1):204–227
- Sumi T, Bennett DP, Bond IA et al. (2010) A Cold Neptune-Mass Planet OGLE-2007-BLG-368Lb: Cold Neptunes Are Common. *ApJ*710(2):1641–1653
- Sumi T, Kamiya K, Bennett DP et al. (2011) Unbound or distant planetary mass population detected by gravitational microlensing. *Nature*473(7347):349–352
- Sumi T, Koshimoto N, Bennett DP et al. (2023) Free-floating Planet Mass Function from MOA-II 9 yr Survey toward the Galactic Bulge. *AJ*166(3):108
- Sutherland AP Fabrycky DC (2016) On the Fate of Unstable Circumbinary Planets: Tatooine’s Close Encounters with a Death Star. *ApJ*818(1):6
- Suzuki D, Bennett DP, Sumi T et al. (2016) The Exoplanet Mass-ratio Function from the MOA-II Survey: Discovery of a Break and Likely Peak at a Neptune Mass. *ApJ*833(2):145
- Suzuki D, Bennett DP, Ida S et al. (2018) Microlensing Results Challenge the Core Accretion Runaway Growth Scenario for Gas Giants. *ApJ*869(2):L34
- Tsapras Y, Hundertmark M, Wyrzykowski Ł et al. (2016) The OGLE-III planet detection efficiency from six years of microlensing observations (2003–2008). *MNRAS*457(2):1320–1331
- Udalski A, Szymański MK Szymański G (2015) OGLE-IV: Fourth Phase of the Optical Gravitational Lensing Experiment. *Acta Astron*65(1):1–38
- Udalski A, Ryu YH, Sajadian S et al. (2018) OGLE-2017-BLG-1434Lb: Eighth $q < 1 \times 10^{-4}$ Mass-Ratio Microlens Planet Confirms Turnover in Planet Mass-Ratio Function. *Acta Astron*68(1):1–42
- van Elteren A, Portegies Zwart S, Pelupessy I, Cai MX McMillan SLW (2019) Survivability of planetary systems in young and dense star clusters. *A&A*624:A120
- Veras D Armitage PJ (2005) The Influence of Massive Planet Scattering on Nascent Terrestrial Planets. *ApJ*620(2):L111–L114
- Veras D Raymond SN (2012) Planet-planet scattering alone cannot explain the free-floating planet population. *MNRAS*421(1):L117–L121

- Veras D, Wyatt MC, Mustill AJ, Bonsor A, Eldridge JJ (2011) The great escape: how exoplanets and smaller bodies desert dying stars. *MNRAS*417(3):2104–2123
- Wang H, Zang W, Zhu W et al. (2022) Systematic Korea Microlensing Telescope Network planetary anomaly search - III. One wide-orbit planet and two stellar binaries. *MNRAS*510(2):1778–1790
- Weidenschilling SJ, Marzari F (1996) Gravitational scattering as a possible origin for giant planets at small stellar distances. *Nature*384(6610):619–621
- Whitworth AP, Zinnecker H (2004) The formation of free-floating brown dwarves and planetary-mass objects by photo-erosion of prestellar cores. *A&A*427:299–306
- Witt HJ, Mao S (1994) Can Lensed Stars Be Regarded as Pointlike for Microlensing by MACHOs? *ApJ*430:505
- Wu Z, Dong S, Yi T et al. (2023) Gaia22dkvLb: A Microlensing Planet Potentially Accessible to Radial-Velocity Characterization. arXiv e-prints arXiv:2309.03944
- Wyrzykowski Ł, Mróz P, Rybicki KA et al. (2020) Full orbital solution for the binary system in the northern Galactic disc microlensing event Gaia16aye. *A&A*633:A98
- Wyrzykowski Ł, Kruszyńska K, Rybicki KA et al. (2023) Gaia Data Release 3. Microlensing events from all over the sky. *A&A*674:A23
- Yan S, Zhu W (2022) Measuring Microlensing Parallax via Simultaneous Observations from Chinese Space Station Telescope and Roman Telescope. *Research in Astronomy and Astrophysics* 22(2):025006
- Yee JC, Gould A, Beichman C et al. (2015) Criteria for Sample Selection to Maximize Planet Sensitivity and Yield from Space-Based Microlens Parallax Surveys. *ApJ*810(2):155
- Yee JC, Zang W, Udalski A et al. (2021) OGLE-2019-BLG-0960 Lb: the Smallest Microlensing Planet. *AJ*162(5):180
- Yoo J, DePoy DL, Gal-Yam A et al. (2004) OGLE-2003-BLG-262: Finite-Source Effects from a Point-Mass Lens. *ApJ*603(1):139–151
- Zang W, Hwang KH, Udalski A et al. (2021) Systematic KMTNet Planetary Anomaly Search. I. OGLE-2019-BLG-1053Lb, a Buried Terrestrial Planet. *AJ*162(4):163
- Zang W, Yang H, Han C et al. (2022) Systematic KMTNet planetary anomaly search. IV. Complete sample of 2019 prime-field. *MNRAS*515(1):928–939
- Zang W, Jung YK, Yang H et al. (2023) Systematic KMTNet Planetary Anomaly Search. VII. Complete Sample of $q < 10^{-4}$ Planets from the First 4 yr Survey. *AJ*165(3):103
- Zhu W, Gould A (2016) Augmenting WFIRST Microlensing with a Ground-Based Telescope Network. *Journal of Korean Astronomical Society* 49(3):93–107
- Zhu W, Udalski A, Novati SC et al. (2017) Toward a Galactic Distribution of Planets. I. Methodology and Planet Sensitivities of the 2015 High-cadence Spitzer Microlens Sample. *AJ*154(5):210